Nucleation and Growth Process of Water Adsorption in Micropores of Activated Carbon Revealed by NMR

Yan Song,[†] Yuan Chong,[‡] Arjun Raghavan,[‡] Yunzhao Xing,[†] Yanchun Ling,[†] Alfred Kleinhammes,[‡] and Yue Wu*[,†,‡]

[†]Department of Applied Physical Sciences and [‡]Department of Physics and Astronomy, University of North Carolina, Chapel Hill, North Carolina 27599-3287, United States

ABSTRACT: Properties of liquids at solid interfaces play a central role in numerous important processes in nature. Nuclear magnetic resonance (NMR) is particularly useful for probing liquid/graphitic carbon interfacial properties. In particular, the nucleus-independent chemical shift (NICS) provides a sensitive measure of the distance between adsorbates and the graphitic carbon surface on the subnanometer scale, enabling NMR to acquire subnanometer scale spatial resolution. Here, by combining the information on thermodynamics obtained from in situ NMR-detected water isotherm and spatially resolved information on structure and dynamics obtained by NICS-resolved NMR, the microscopic process of water nucleation and growth inside the micropore of activated carbons is investigated. The formation of water clusters at surface sites, the cooperative growth process of pore bridging, and the final stage of horizontal pore filling are revealed in detail, demonstrating the potential of this comprehensive NMR approach for studying microscopic mechanisms at solid/liquid interfaces including electrochemical processes.

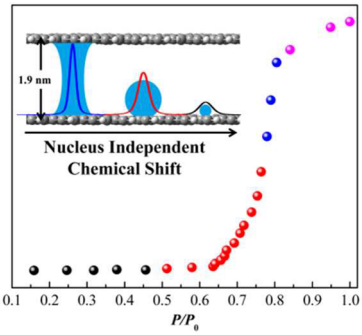

1. INTRODUCTION

Understanding physicochemical properties of water at interfaces is of crucial importance for developing novel technologies and applications.[1] Although various analytical methods such as XPS,[2] AFM,[3] STM,[4] and so on have been used to study the aqueous interfaces, these techniques are not suitable for studying adsorbed water inside complex porous networks due to the difficulty of accessing the inside of pores. In contrast, NMR is well-suited for probing local structures and dynamics of water adsorbed or confined inside porous media.[5−10] NMR is very sensitive to local environments, with distinct ability in acquiring atomic-scale information on adsorbed species.[11,12] In particular, for graphitic carbon surface, there is a quantitative relationship between an extra chemical shift δ_{NICS}, called the nucleus-independent chemical shift, and the distance of the nucleus to the graphitic carbon surface.[13−15] Such δ_{NICS} ↔ distance relationship provides NMR with very valuable spatial resolution near graphitic carbon surface.

In this work, such NICS NMR approach is employed to study microscopic processes of water adsorption inside activated carbon micropores (defined as pores with surface-to-surface pore size ≤2 nm). Although previous experimental studies investigated the mechanism of water adsorption in activated carbon, they rely primarily on the water adsorption isotherm that lacks direct local structural information.[16−30] Molecular dynamics simulations offered clues on the microscopic adsorption mechanisms.[22−27] However, direct experimental validations of these proposed water adsorption mechanisms are scarce. In this work, the subnanometer scale spatial information on nucleated water clusters in different stages of adsorption levels are obtained using the NICS NMR method. Combined with NMR-detected water adsorption isotherm, details of the nucleation and growth processes of water inside activated carbon micropores are revealed.

2. EXPERIMENTAL SECTION

2.1. Synthesis of Microporous Activated Carbon. The sample studied is an activated carbon derived from the high-temperature polymer, polyether ether ketone (PEEK).[31] The sample preparation process consists of two steps: carbonization and activation. During carbonization, 2 g of granulated Victrex PEEK is heated in an argon gas tube at 900 °C for 30 min, yielding the carbonized product. Then, the product is cooled to room temperature in an argon environment and ground into smaller particles. During the activation, water steam is introduced to enlarge the micropores created during carbonization. The ground carbonized sample is oxidized at 900 °C under the water steam, carried by the Ar gas flow, for a certain time period. Different activation times lead to different mass loss amounts and micropore sizes. In this study, the sample (labeled as PEEK-90) is heated until 90% of the mass is lost; this mass loss refers to the ratio between the sample mass after activation and that before activation but after carbonization.

2.2. NMR Experiments. All ^{1}H magic-angle spinning (MAS) NMR spectra are obtained at 400 MHz, under MAS spinning speed of 8 kHz, and at room temperature (T = 296

Received: March 4, 2017
Revised: March 24, 2017
Published: April 6, 2017

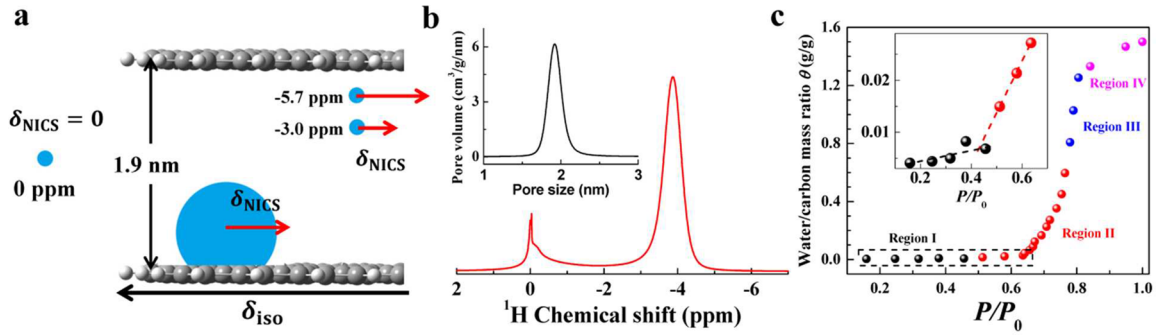

Figure 1. (a) Illustration of molecules inside a slit-shaped pore of width 1.9 nm (carbon atom center to center). The gray spheres are carbon atoms, and the blue spheres represent water clusters. (b) ^{1}H MAS NMR spectra of water in the PEEK-90 activated carbon sample. The chemical shift of the free water outside the pore (left peak) is set to 0 ppm. The inset of panel b is the pore size distribution of PEEK-90. (c) NMR-detected adsorption isotherm of water in PEEK-90. The curve is divided into four regions according to the water−carbon mass ratio θ. Black: $\theta < 0.01$, region I; red: $0.01 < \theta < 0.60$, region II; blue: $0.60 < \theta < 1.25$, region III; purple: $1.25 < \theta < 1.50$, region IV. The region in the dashed box is magnified in the inset of panel c, showing the onset of cooperative adsorption at water relative pressure of $P/P_0 = 0.5$ ($\theta = 0.01$).

K). Before NMR measurement, 15 mg of PEEK-90 sample is loaded into a 4 mm MAS NMR rotor and dried at 90 °C in vacuum for 24 h to remove preadsorbed water. Then, a background ^{1}H NMR spectrum of the vacuum-treated PEEK-90 is first recorded, showing a weak, broad peak of 40 ppm (full width at half-maximum (FWHM)) that is then subtracted from all presented spectra. Varying amounts of water vapor are added by placing the sample in a saturated water vapor system at 296 K for proportional durations. The amount of water loaded is determined by finding the mass difference between the vapor-loaded sample and the initial, dry sample. A single-pulse excitation with pulse duration of 5 μs and a 5 s relaxation delay is applied. The longitudinal relaxation time (T_1) is measured by the standard inversion−recovery method (pulse sequence 180°−τ−90°).

2.3. Water Isotherm. An in situ NMR-based method is used to measure the water isotherm of the PEEK-90 sample. Detailed descriptions of the instrument can be found in Chong et al.[32] The water adsorption isotherm at 296 K is measured at ^{1}H frequency of 34.3 MHz. The ^{1}H free-induction-decay (FID) signal of the dry sample is first acquired by a single-pulse excitation with pulse duration of 8 μs. A broad peak of 750 ppm (FWHM) is observed in the background spectrum and is subtracted from subsequent spectra. Water vapor is then loaded to the sample at varying vapor pressures, and the NMR spectra of the hydrated samples are acquired. The loaded water mass is determined as follows: total water mass at saturation is found by direct weighing; then, the presaturation masses are determined by comparing the corresponding peak intensities to the saturation peak intensity. The adsorption isotherm is obtained by plotting the water−carbon mass ratio as a function of relative vapor pressure.

3. RESULTS AND DISCUSSION

NICS originates from delocalized π electron orbitals in graphitic-like carbon surface, giving rise to a diamagnetic response and reducing the local magnetic field at the nucleus near the graphitic carbon surface. Density functional theory (DFT) calculations show that the NICS value of a nucleus increases rapidly as the distance of the nucleus and the carbon surface decreases, especially within the range of a nanometer.[13] The NICS value δ_{NICS} can be expressed as a function of the distance r between the probe atom and the carbon surface (atomic center to center)

$$\delta_{NICS}(r) = A \exp\left[-\left(\frac{r}{r_0}\right)^{\beta}\right] + A \exp\left[-\left(\frac{d-r}{r_0}\right)^{\beta}\right] \quad (1)$$

with the parameters $A = -24.5$ ppm, $r_0 = 0.227$ nm, and $\beta = 0.754$; d is the width of the slit-shaped pore (atomic center to center).[13] For a single nucleus inside a slit-shaped pore of 1.9 nm in width (atomic center to center), as illustrated in Figure 1a, the δ_{NICS} of the nucleus is −5.7 ppm if it is 0.4 nm away from the surface (from the carbon atom center to the probing nucleus), while at a distance of 0.7 nm, $\delta_{NICS} = -3.0$ ppm ($\delta_{NICS} = 0$ ppm for nucleus outside the pore). Thus several angstroms difference in position can cause a significant difference in δ_{NICS}, enabling NMR to evaluate the distance of the nucleus from the surface. For a molecular cluster that is liquid-like, motional averaging has to be considered in calculating the measured average δ_{NICS}. For example, as shown in Figure 1a, a group of molecules form a cluster in which molecules move rapidly on the NMR time scale (~10 ms) within the cluster. The measured δ_{NICS} is then the average of the δ_{NICS} values of all nuclear spins within the cluster. Additionally, it is worth noting that the measured δ_{NICS} cannot average over water in different micropores. As shown in Figure S1 (Supporting Information), on the NMR time scale and even over longer durations (20 ms), the ^{1}H NMR 2D exchange experiment shows there is no exchange between water in different micropores and also no exchange between water in micropores and water in larger mesopores and in intergranular space.

Figure 1b shows the ^{1}H MAS NMR spectrum of PEEK-90 activated carbon sample fully filled with water ($\theta = 2.38$). The left peak set at 0 ppm is due to water in the intergranular space (sharp peak) and large mesopores (broad shoulder); the right peak at −3.9 ppm is due to water inside micropores.[5] The pore size distribution of PEEK-90 is obtained by NMR NICS analysis and is shown in the inset of Figure 1b.[13] On the basis of this analysis the average pore size (carbon atom center to center) of the PEEK-90 activated carbon sample is 1.90 nm. More importantly, the FWHM of the distribution is only 0.20 nm, showing that the pore size of the PEEK-90 activated carbon sample is rather uniform. The water adsorption isotherm at 296 K is measured at ^{1}H frequency of 34.3 MHz equipped with an in situ water loading system under controlled relative water vapor pressure P/P_0. As shown in Figure 1c, the

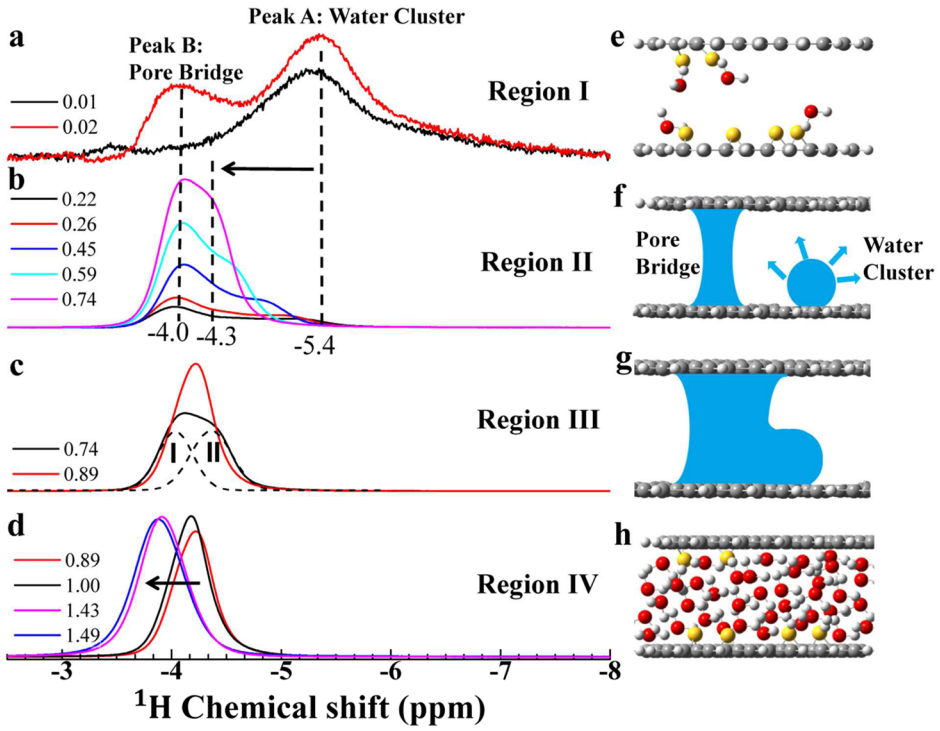

Figure 2. (a–d) ^{1}H MAS NMR spectra of water adsorbed in PEEK-90 activated carbon at different θ, ranging from 0 to 1.49. Varying amounts of water are added by placing the sample in a saturated water vapor system at room temperature for different durations; greater adsorption levels require longer durations in the water vapor system. (e–h) Schematic diagrams of water adsorption structures in activated carbon at different filling levels. The gray spheres are carbon atoms, the yellow spheres represent surface adsorption sites, the red spheres represent O, and the white spheres represent H.

adsorption isotherm of water in PEEK-90 is a typical Type V curve according to the IUPAC classification.[33] The isotherm is divided into four regions according to the information provided by the NICS-resolved NMR, which will be discussed below.

Figure 2a shows the ^{1}H MAS NMR spectra for the two lowest water filling levels. At the water–carbon mass ratio θ = 0.01, the spectrum (black curve) consists only of a single broad peak, labeled as peak A. The NICS of peak A is −5.4 ppm and is the most negative among all spectra studied. As discussed above, the measured chemical shift is the average of the δ_{NICS} values of all protons within the water cluster. A simple model is applied to correlate the measured δ_{NICS} with the height of adsorbed water cluster. Here it is assumed that the density spatial distribution (ρ) of water molecules throughout the water cluster is uniform; that is, the number of water molecules inside the cluster at each height is identical. For a slit-shaped pore of width 1.9 nm (PEEK-90), the averaged δ_{NICS}, δ_{avg}, of such adsorbed water cluster can be calculated as

$$\delta_{avg} = \frac{\int_{0.32}^{h+0.17} \rho(r)\delta(r)\,dr}{\int_{0.32}^{h+0.17} \rho(r)\,dr} \quad (2)$$

where h is the height of adsorbed water cluster, 0.17 nm is the radius of a carbon atom, 0.32 nm is the closest distance between a hydrogen atom and the carbon atom, r is the distance between the hydrogen atom center and the graphitic-like carbon surface (atomic center to center), and $\rho(r)$ is the density spatial distribution of the water cluster (assumed to be constant in this model).[34] Because the δ_{avg} of peak A equals −5.4 ppm, the height h of adsorbed water cluster for peak A is 0.35 nm, which is in good agreement with the height of a monolayer water (0.37 nm).[3] Therefore, it can be concluded that water molecules associated with peak A are, on average, directly adsorbed on the carbon surface. Because water molecules do not have affinity to the hydrophobic carbon surface, they tend to nucleate at hydrophilic defect sites, usually oxygen-containing functional groups, via hydrogen bonding.[35] The broad ^{1}H NMR spectrum of peak A is a result of both the restricted mobility of the water molecules and the differences in chemical environments of water at defect sites. Such surface site nucleation process is depicted in Figure 2e. Moreover, compared with the isotherm (Figure 1c) at θ < 0.01, this spectrum corresponds to the initial adsorption region I of the isotherm (P/P_0 < 0.5 and θ < 0.01, black dots). The amount of adsorbed water in region I is very small, indicating that the density of surface adsorption sites in the PEEK-90 sample is very low. There are very few surface sites for water to nucleate.[17]

When θ is increased slightly to 0.02 (red curve in Figure 2a), corresponding to the adsorption region II in the isotherm, two well-resolved peaks are clearly observed. One peak is broad and located at −5.4 ppm, having the same shift and shape as peak A for θ = 0.01, indicating a similar water cluster size. The other peak (peak B) is narrower and is located at −4.0 ppm. Peak B has a less negative δ_{avg} than peak A, indicating that the average distance of water molecules associated with peak B is larger than that of peak A. Upon further increase of θ up to 0.74 (Figure 2b), spectra continue to show two well-resolved peaks. However, these two peaks vary markedly differently with increasing θ. Peak B does not shift, staying constant at about −4.0 ppm, while peak A gradually shifts from −5.4 ppm to −4.3 ppm. To analyze peak B, two distinct features of the spectrum are considered. First, the δ_{avg} of peak B is always at −4.0 ppm as

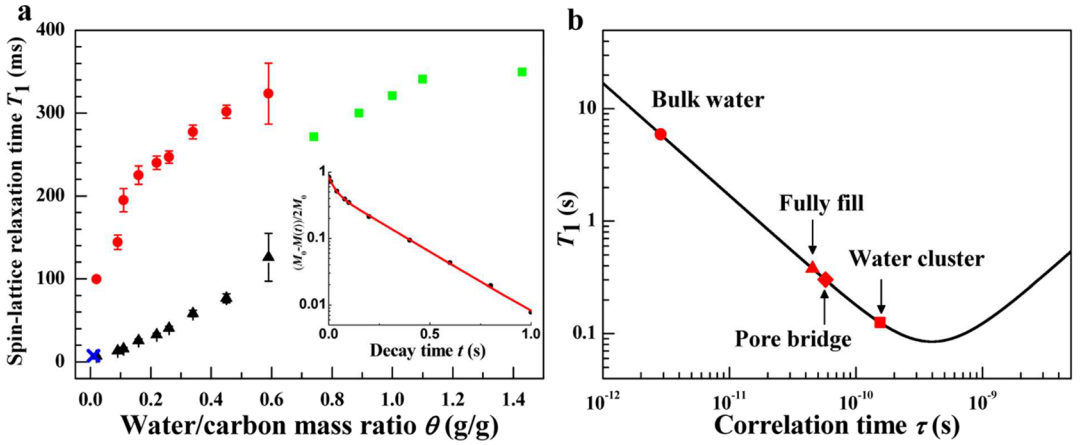

Figure 3. (a) ^{1}H spin−lattice relaxation time (T_1) of adsorbed water in different stages of water adsorption. Blue cross: θ = 0.01, region I; black triangles: surface clusters; red spheres: pore bridges; green squares: single peak region with nearly filled pores, regions III and IV. The standard deviations of the T_1 fitting are given by the error bars. The inset is the ^{1}H magnetization decay curve at θ = 0.16. The solid line is a fit using the double-exponential function. (b) Theoretical value of T_1 based on intramolecular dipolar interaction. The correlation times of bulk water, water in the fully filled PEEK-90 sample, pore bridge, and water cluster at θ = 0.59 are 3.5, 49, 53, and 154 ps, respectively.

the amount of adsorbed water increases. Second, the δ_{avg} of peak B (−4.0 ppm) is very close to the δ_{avg} of fully filled sample, which is at −3.9 ppm. This indicates that the average distance of water clusters associated with peak B does not change with increasing θ. This suggests that water molecules associated with peak B form bridges across the opposing pore walls, spanning the height of the micropore (Figure 2f). The formation of pore bridges is a more cooperative process compared with nucleation at surface sites. The onset of cooperative bridging depends on the local density of surface defect sites, as suggested by previous simulation results.[23,24,36] In regions with denser defect sites, the opportunity for cooperative adsorption is high; a few water molecules could form more hydrogen bonds with neighboring adsorbed water molecules by forming bridges across the pores. This cooperative adsorption process is energetically favorable, leading to a significantly enhanced adsorption with small changes in the relative water vapor pressure P/P_0. While the shift of peak B stays constant, peak A gradually shifts to the left as θ increases, signifying that on average water molecules are moving farther away from the carbon surface. Because, as mentioned above, peak A corresponds to water clusters adsorbed on the surface adsorption sites, the shift of peak A must be a result of the growth of water clusters at these sites. Eventually, the clusters grow large enough such that the NICS of peak A approaches that of peak B. Different from peak B, water molecules associated with peak A are in regions with sparse surface sites; they have less chance of bridging across the pores and their sizes grow gradually with a gradually shifting NICS rather than jumping immediately to −4.0 ppm. As illustrated in Figure 2f, water adsorption at this intermediate filling stage is controlled by two parallel processes: the cluster growth and the cooperative pore bridging. Compared with the isotherm in Figure 1c, this stage corresponds to region II of 0.5 < P/P_0 < 0.75 and 0.01 < θ < 0.60 (red dots). In the inset of Figure 1c, the amount of adsorbed water in region II increases much faster than in region I. Thus cooperativity of pore bridging plays an important role in the adsorption process.

When θ is increased to 0.89 (Figure 2c), the ^{1}H MAS NMR spectra are again dominated by a single peak. Comparing the spectra of θ = 0.89 and θ = 0.74 in Figure 2c, it is evident that the peak center of θ = 0.89 is located in between the peak centers of the θ = 0.74 spectrum. The disappearance of the two peaks is due to the coalescence of pore bridges and water clusters. In earlier stages, pore bridges and water clusters are spatially separated and unconnected, which is supported by the lack of exchange in the 2D exchange NMR shown in Figure S2 (Supporting Information). Thus the NMR spectra display two different peaks: one for the bridges and the other for the clusters. However, when the pore bridges and water clusters become connected to additional water adsorption, the peaks from distinct chemical environments finally merge and the NMR spectra display a single peak. As illustrated in Figure 2g, the newly adsorbed water fills empty space between water clusters and pore bridges, connecting clusters and bridges. This interpretation is supported by the following estimation. The spectrum of θ = 0.74 can be fitted by two individual Gaussian peaks, peak I and peak II (dashed lines in Figure 2c). Peaks I and II represent pore bridges and water clusters, respectively. The peak centers of peak I and peak II are −4.03 and −4.36 ppm, respectively. Assuming a symmetric exchange between the two peaks, the peak center of the exchange spectrum is equal to −4.19 ppm. This value is in very good agreement with the experimentally observed chemical shift of −4.2 ppm when θ = 0.89. Compared with the isotherm in Figure 1c, this stage corresponds to region III of 0.75 < P/P_0 < 0.80 and 0.80 < θ < 1.25 (blue dots). The amount of adsorbed water in region III increases even steeper than in region II. In this stage, the adsorption is mainly controlled by the coalescence of water clusters and pore bridges.

In Figure 2d, the single peak gradually shifts to the left upon further adsorption because water starts to fill some remaining empty space, inducing horizontal pore filling along the pores (see Figure 2h).[30,31] As θ reaches 1.49, no more water can be absorbed, indicating that the micropores in PEEK-90 have been fully filled by water. Compared with the isotherm, this stage corresponds to region IV of 0.80 < P/P_0 ≤ 1 and 1.25 < θ < 1.50 (purple dots). The amount of adsorbed water in region IV is small because most of the pores have been filled already.

The dynamics of adsorbed water molecules is investigated by measuring the ^{1}H spin−lattice relaxation times (T_1) via the standard inversion−recovery method. Assuming that the ^{1}H T_1

relaxation process in water is dominated by the fluctuations of intramolecular proton−proton dipolar interaction, T_1 is given by

$$\left(\frac{1}{T_1}\right) = \frac{3\mu_0^2\gamma^4\hbar^2}{160\pi^2 r^6}\left(\frac{\tau}{1+\omega_0^2\tau^2} + \frac{4\tau}{1+4\omega_0^2\tau^2}\right) \quad (3)$$

where γ is the gyromagnetic ratio of proton, $2\pi\hbar$ is the Planck constant, $r = 0.156$ nm is the distance between the two protons in a water molecule, μ_0 is the magnetic permeability of free space, τ is the rotational correlation time, and $\omega_0/2\pi$ is the Larmor frequency (400 MHz).[37] The rotational correlation time τ is estimated by the average time taken for the molecule to rotate by 1 rad.[38] Small τ corresponds to fast molecular motion, while large τ corresponds to slow molecular motion.

Figure 3 shows the ^{1}H T_1 of confined water in different stages of water adsorption. In the surface site nucleation stage ($\theta = 0.01$, region I), the decay curve can be fitted very well with a single exponential decay $M(t)/M_0 = 1 - 2\exp(-t/T_1)$, where M is the magnetization of ^{1}H nuclei and M_0 is the equilibrium magnetization. A very short T_1 of 8 ms is observed (blue cross in Figure 3a). This T_1 is significantly shorter than the value of bulk water (several seconds) and also shorter than the value of water in fully filled micropores (several hundred milliseconds). Such a short T_1 value is caused by the slowdown of water molecular motion. In the beginning, few water molecules nucleate on surface sites, forming water clusters that are quite different from bulk-water-like network. In these surface-nucleation water clusters, the molecular motions, such as rotation and translation, are highly restricted by surface sites, making the rate of molecular motion slow down and causing effective spin−lattice relaxation with short T_1.[37]

In the cooperative filling stage (region II), two different T_1 values are observed. Specifically, the T_1 value of the water clusters increases from 10 to 110 ms. In the meantime, the T_1 value of the pore bridges increases from 100 to 330 ms. The inset in Figure 3a shows a typical ^{1}H magnetization decay curve in region II ($\theta = 0.16$). It clearly shows two components of exponential decays and can be fitted very well with a double-exponential function (red solid line). Finally, in the final stage (region III and IV) where the two peaks merge together, there is only a single T_1 reaching a plateau around 350 ms, which is the typical T_1 value for water of filled micropores. Similar T_1 behaviors have been reported by Wang[17] and Khozina.[39]

In contrast with the surface site nucleation stage, both water clusters and pore bridges in the cooperative and final filling stages contain more water molecules with more developed hydrogen network. Therefore, eq 3 is applied to estimate the corresponding correlation times based on the measured T_1. Figure 3b plots the theoretical values of T_1 versus τ. According to the adsorption model, the pore bridging region is similar to the fully filled micropore, predicting that the correlation times of these two structures should be similar. Moreover, because of the less developed hydrogen network, the motion of water molecules in water cluster is slower than in pore bridges. Thus the correlation time τ of water clusters should be longer than that of pore bridges. Both predictions are confirmed by the experimental results. As shown in Figure 3b, the τ of fully filled sample ($\theta = 1.49$) is 49 ps, very similar to the $\tau = 53$ ps of pore bridges. The τ of water clusters is 154 ps, which, as expected, is much longer than that of pore bridges.

4. CONCLUSIONS

This study showcases the unique power of NICS-based NMR to probe the intricacies of confined fluid−solid interactions on the nanometer scale. While previous research had focused on isotherms, which only provide information on the amount of adsorption, the present measurement directly images how the water clusters nucleate and grow during the adsorption process. This study provides direct experimental evidence of the detailed nucleation and growth processes of water inside activated carbon micropores. It is shown that water adsorption starts with nucleation at surface sites. This is followed by two growth processes. One is the gradual growth of water clusters, and the other is the cooperative growth by pore-bridging. These two processes both contribute to the water adsorption associated with the sharp increase in the water isotherm. Finally, these two distinct water structures coalesce together, leading to the pore filling along the pores in the final stage. Future studies can make use of this NICS-based NMR method to study molecular and ionic processes nanoconfined by graphitic-like carbon surfaces.

■ ASSOCIATED CONTENT

Supporting Information

The Supporting Information is available free of charge on the ACS Publications website at DOI: 10.1021/acs.jpcc.7b02093.

^{1}H 2D-exchange spectroscopy (EXSY) NMR (PDF)

■ AUTHOR INFORMATION

Corresponding Author

*E-mail: yuewu@physics.unc.edu.

ORCID

Yue Wu: 0000-0002-7440-0512

Notes

The authors declare no competing financial interest.

■ ACKNOWLEDGMENTS

This work is supported by UNC Kenan Research fund.

■ REFERENCES

(1) Björneholm, O.; Hansen, M. H.; Hodgson, A.; Liu, L.-M.; Limmer, D. T.; Michaelides, A.; Pedevilla, P.; Rossmeisl, J.; Shen, H.; Tocci, G.; et al. Water at Interfaces. *Chem. Rev.* **2016**, *116*, 7698−7726.

(2) Ogasawara, H.; Brena, B.; Nordlund, D.; Nyberg, M.; Pelmenschikov, A.; Pettersson, L. G. M.; Nilsson, A. Structure and Bonding of Water on Pt(111). *Phys. Rev. Lett.* **2002**, *89*, 276102.

(3) Xu, K.; Cao, P.; Heath, J. R. Graphene Visualizes the First Water Adlayers on Mica at Ambient Conditions. *Science* **2010**, *329*, 1188−1191.

(4) Mitsui, T.; Rose, M. K.; Fomin, E.; Ogletree, D. F.; Salmeron, M. Water Diffusion and Clustering on Pd(111). *Science* **2002**, *297*, 1850−1852.

(5) Luo, Z.-X.; Xing, Y.-Z.; Ling, Y.-C.; Kleinhammes, A.; Wu, Y. Electroneutrality breakdown and specific ion effects in nanoconfined aqueous electrolytes observed by NMR. *Nat. Commun.* **2015**, *6*, 6358.

(6) Luo, Z.-X.; Xing, Y.-Z.; Liu, S.; Ling, Y.-C.; Kleinhammes, A.; Wu, Y. Dehydration of Ions in Voltage-Gated Carbon Nanopores Observed by in Situ NMR. *J. Phys. Chem. Lett.* **2015**, *6*, 5022−5026.

(7) Wang, H.-J.; Xi, X.-K.; Kleinhammes, A.; Wu, Y. Temperature-Induced Hydrophobic-Hydrophilic Transition Observed by Water Adsorption. *Science* **2008**, *322*, 80−83.

(8) Griffin, J. M.; Forse, A. C.; Tsai, W.-Y.; Taberna, P.-L.; Simon, P.; Grey, C. P. In situ NMR and Electrochemical Quartz Crystal

Microbalance Techniques Reveal the Structure of the Electrical Double Layer In Supercapacitors. *Nat. Mater.* **2015**, *14*, 812−819.
(9) Forse, A. C.; Griffin, J. M.; Merlet, C.; Bayley, P. M.; Wang, H.; Simon, P.; Grey, C. P. NMR Study of Ion Dynamics and Charge Storage in Ionic Liquid Supercapacitors. *J. Am. Chem. Soc.* **2015**, *137*, 7231−7242.
(10) Griffin, J. M.; Forse, A. C.; Grey, C. P. Solid-state NMR Studies of Supercapacitors. *Solid State Nucl. Magn. Reson.* **2016**, *74*−*75*, 16−35.
(11) Yuzawa, H.; Aoki, M.; Itoh, H.; Yoshida, H. Adsorption and Photoadsorption States of Benzene Derivatives on Titanium Oxide Studied by NMR. *J. Phys. Chem. Lett.* **2011**, *2*, 1868−1873.
(12) Huang, S.-J.; Hung, C.-T.; Zheng, A.; Lin, J.-S.; Yang, C.-F.; Chang, Y.-C.; Deng, F.; Liu, S.-B. Capturing the Local Adsorption Structures of Carbon Dioxide in Polyamine-Impregnated Mesoporous Silica Adsorbents. *J. Phys. Chem. Lett.* **2014**, *5*, 3183−3187.
(13) Xing, Y.-Z.; Luo, Z.-X.; Kleinhammes, A.; Wu, Y. Probing Carbon Micropore Size Distribution by Nucleus Independent Chemical Shift. *Carbon* **2014**, *77*, 1132−1139.
(14) Forse, A. C.; Griffin, J. M.; Presser, V.; Gogotsi, Y.; Grey, C. P. Ring Current Effects: Factors Affecting the NMR Chemical Shift of Molecules Adsorbed on Porous Carbons. *J. Phys. Chem. C* **2014**, *118*, 7508−7514.
(15) Merlet, C.; Forse, A. C.; Griffin, J. M.; Frenkel, D.; Grey, C. P. Lattice Simulation Method to Model Diffusion and NMR Spectra in Porous Materials. *J. Chem. Phys.* **2015**, *142*, 094701.
(16) Furmaniak, S.; Gauden, P. A.; Terzyk, A. P.; Rychlicki, G. Water Adsorption on Carbons-Critical Review of the Most Popular Analytical Approaches. *Adv. Colloid Interface Sci.* **2008**, *137*, 82−143.
(17) Wang, H.-J.; Kleinhammes, A.; McNicholas, T. P.; Liu, J.; Wu, Y. Water Adsorption in Nanoporous Carbon Characterized by in Situ NMR: Measurements of Pore Size and Pore Size Distribution. *J. Phys. Chem. C* **2014**, *118*, 8474−8480.
(18) Horikawa, T.; Sekida, T.; Hayashi, J. I.; Katoh, M.; Do, D. D. A New Adsorption−Desorption Model for Water Adsorption in Porous Carbons. *Carbon* **2011**, *49*, 416−424.
(19) Do, D. D.; Junpirom, S.; Do, H. D. A New Adsorption−Desorption Model for Water Adsorption in Activated Carbon. *Carbon* **2009**, *47*, 1466−1473.
(20) Do, D. D.; Do, H. D. A Model for Water Adsorption in Activated Carbon. *Carbon* **2000**, *38*, 767−773.
(21) Tao, Y.; Endo, M.; Kaneko, K. Hydrophilicity-Controlled Carbon Aerogels with High Mesoporosity. *J. Am. Chem. Soc.* **2009**, *131*, 904−905.
(22) Brennan, J. K.; Thomson, K. T.; Gubbins, K. E. Adsorption of Water in Activated Carbons: Effects of Pore Blocking and Connectivity. *Langmuir* **2002**, *18*, 5438−5447.
(23) McCallum, C. L.; Bandosz, T. J.; McGrother, S. C.; Müller, E. A.; Gubbins, K. E. A Molecular Model for Adsorption of Water on Activated Carbon: Comparison of Simulation and Experiment. *Langmuir* **1999**, *15*, 533−544.
(24) Müller, E. A.; Rull, L. F.; Vega, L. F.; Gubbins, K. E. Adsorption of Water on Activated Carbons: A Molecular Simulation Study. *J. Phys. Chem.* **1996**, *100*, 1189−1196.
(25) Ohba, T.; Kanoh, H.; Kaneko, K. Affinity Transformation from Hydrophilicity to Hydrophobicity of Water Molecules on the Basis of Adsorption of Water in Graphitic Nanopores. *J. Am. Chem. Soc.* **2004**, *126*, 1560−1562.
(26) Ohba, T.; Kanoh, H.; Kaneko, K. Water Cluster Growth in Hydrophobic Solid Nanospaces. *Chem. - Eur. J.* **2005**, *11*, 4890−4894.
(27) Ohba, T.; Kanoh, H.; Kaneko, K. Cluster-Growth-Induced Water Adsorption in Hydrophobic Carbon Nanopores. *J. Phys. Chem. B* **2004**, *108*, 14964−14969.
(28) Striolo, A.; Gubbins, K. E.; Gruszkiewicz, M. S.; Cole, D. R.; Simonson, J. M.; Chialvo, A. A.; Cummings, P. T.; Burchell, T. D.; More, K. L. Effect of Temperature on the Adsorption of Water in Porous Carbons. *Langmuir* **2005**, *21*, 9457−9467.
(29) Mahle, J. J. An Adsorption Equilibrium Model for Type 5 Isotherms. *Carbon* **2002**, *40*, 2753−2759.
(30) Talu, O.; Meunier, F. Adsorption of Associating Molecules in Micropores and Application to Water on Carbon. *AIChE J.* **1996**, *42*, 809−819.
(31) McNicholas, T. P.; Wang, A.; O'Neill, K.; Anderson, R. J.; Stadie, N. P.; Kleinhammes, A.; Parilla, P.; Simpson, L.; Ahn, C. C.; Wang, Y.; et al. H_2 Storage in Microporous Carbons from PEEK Precursors. *J. Phys. Chem. C* **2010**, *114*, 13902−13908.
(32) Chong, Y.; Kleinhammes, A.; Tang, P.; Xu, Y.; Wu, Y. Dominant Alcohol-Protein Interaction via Hydration-Enabled Enthalpy-Driven Binding Mechanism. *J. Phys. Chem. B* **2015**, *119*, 5367−5375.
(33) Sing, K. S. W. Reporting Physisorption Data for Gas/Solid Systems with Special Reference to the Determination of Surface Area and Porosity (Recommendations 1984). *Pure Appl. Chem.* **1985**, *57*, 603−619.
(34) Anderson, R. J.; McNicholas, T. P.; Kleinhammes, A.; Wang, A.; Liu, J.; Wu, Y. NMR Methods for Characterizing the Pore Structures and Hydrogen Storage Properties of Microporous Carbons. *J. Am. Chem. Soc.* **2010**, *132*, 8618−8626.
(35) Brennan, J. K.; Bandosz, T. J.; Thomson, K. T.; Gubbins, K. E. Water in Porous Carbons. *Colloids Surf., A* **2001**, *187*−*188*, 539−568.
(36) Jorge, M.; Schumacher, C.; Seaton, N. A. Simulation Study of the Effect of the Chemical Heterogeneity of Activated Carbon on Water Adsorption. *Langmuir* **2002**, *18*, 9296−9306.
(37) Abragam, A. *The Principles of Nuclear Magnetism*; Clarendon Press: Oxford, U.K., 1961.
(38) Levitt, M. H. *Spin Dynamics: Basics of Nuclear Magnetic Resonance*; John Wiley & Sons: 2001.
(39) Gogelashvili, G. S.; Vartapetyan, R. S.; Ladychuk, D. V.; Grunin, Y. B.; Khozina, E. V. Specific Features of the Adsorption and Nuclear Magnetic Relaxation of the Water Molecules in Active Carbons: 2. The State of Water in Active Carbon with Relatively Large Pores According to the NMR Relaxation Data. *Colloid J.* **2004**, *66*, 271−276.